11th International Conference on Fracture Mechanics of Concrete and Concrete Structures
FraMCoS-11
J. M. Chandra Kishen, A. Ramaswamy, S. Ray and R. Vidyasagar (Eds)
https://doi.org/10.21012/FC11.0923109

EXPERIMENTAL STUDY: FRACTURE PROPERTIES OF FLY ASH-SLAG BASED GEOPOLYMER CONCRETE

RAJEEV KUMAR RANJAN[1*] AND ANANTH RAMASWAMY[1†]

[1]Department of Civil Engineering
Indian Institute of Science, Bangalore-560012, India
[*]e-mail: rajeevranjan@iisc.ac.in
[†]e-mail: ananth@iisc.ac.in

Key words: GPC, Load-CMOD, Fracture Energy, 3-Point Bending Test, Micro-characterization.

Abstract: Geopolymer concrete (GPC), also termed as Alkali activated material is an innovative and green concrete, serving as an alternative to the ordinary Portland cement (OPC) concrete. This study aims to investigate the flexural behavior of geopolymer concrete to better understand the mechanical properties and potential application in structural engineering. This research involves the formulation of geopolymer mixes using various binder compositions, incorporating different types of aggregates, and curing at ambient conditions. The experimental program includes 3-point bending tests on the prismatic geopolymer specimens to evaluate their flexural strength, load-CMOD, and cracking behavior. Additionally, the effect of GGBFS content in GPC has been studied. The results of the study revealed that geopolymer concrete exhibits considerable flexural strength comparable to the OPC concrete.

1 INTRODUCTION

In recent years, there has been growing concern about the environmental impact of cement production, prompting researchers and engineers to seek sustainable alternatives. Concrete industry has been playing a significant role in achieving the goals of The Paris agreement by introducing different measures. Carbon capturing and storage of CO_2 and partial or complete replacement of cement clinker are some of the major steps which will help in the reduction of CO_2 emission from production of OPC concrete. Additionally, the disposal of industrial waste like fly ash, GGBFS, red mud, metakaolin, rice husk is a challenging task. Alkali activated cementitious materials, also termed as geopolymer binders have gained significant attention in the past two decades in order to reduce the consumption of cement in concrete industry and further, solve the problems of disposal of industrial wastes. By utilising the industrial wastes as precursors in the alkali activated material, 80 % of the CO_2 emitted from the cement industries can be reduced [1]. Geopolymers concrete is an innovative type of concrete which is produced by the alkali activation of material rich in aluminosilicates [2]. Structurally, these are amorphous to crystalline 3-D silico-aluminate framework [2]. Previous studies have shown that an optimally designed geopolymer concrete bears better mechanical properties and durability as compared to OPC based concrete [3-6]. Many researchers have studied the microstructural aspects of geopolymer concrete using SEM, XRD, and FT-IR and concluded that it possesses dense interfacial transition zone (ITZ) around the aggregates [7-9].

Table 1: Oxide composition of precursor (%)

Precursor	Al_2O_3	SiO_2	CaO	Fe_2O_3	MgO	SO_3	MnO	TiO_2
GGBFS	17.92	34.81	37.63	0.66	7.8	0.2	0.21	-
Fly ash	20.3	59.3	5.88	7.11	0.281	0.838	0.0836	1.74

Table 2: Properties of aggregates

Types of aggregates	WA	SG	EI (%)	FI (%)
20 mm	0.55	2.68	23.13	18.13
10 mm	0.57	2.65	1.22	5.36
M-sand	2.01	2.69	N.A.	N.A.

WA- water absorption, SG- Specific gravity
EI- Elongation Index, FI- Flakiness index.

Very few literatures have been found on the fracture properties of geopolymer concrete. This study investigates fresh properties, fracture properties of geopolymer concrete and focusses on
the micro-characterisation of the precursor and hardened GPC.

2 EXPERIMENTAL METHODS

2.1 Materials

Class F type fly ash (as per ASTM618-08 specification) obtained from the local Bellari thermal power plant in Karnataka, India, and the GGBFS procured from JSW company, are used as a precursor in mix-design. XRF technique has been used to find the percentage composition of fly ash and GGBFS as shown in Table 1. The M-sand is used as fine aggregates, while 10 mm and 20 mm aggregates are used as coarse aggregates Their properties are listed in Table 2. In this study, the percentage of fly ash and GGBFS is chosen as 70% and 30%, respectively for mix-1; 50% and 50%, respectively for mix-2 design. The mix design of the GPC has been listed in Table 3. A combination of sodium hydroxide and sodium silicate is used as a activator solution. The molarity of NaOH is 12M and a ratio of 1.5 for sodium silicate to sodium hydroxide (R) has been used in the mix.
Naphthalene based superplasticizer is used 2% by mass of binder to enhance the workability of concrete.

2.2 Details of specimen preparation and Experimental setup

2.2.1 Specimen Preparation

The precursor materials, fine aggregates, coarse aggregates, and alkaline solutions are mixed in pan mixture. Initially precursor materials, fine aggregates and coarse aggregates are mixed for 2-3 minutes. After that, alkaline solutions and superplasticizer are mixed for 6-7 minutes. After mixing, concrete mixtures were poured in the wooden beam mould, iron cube mould and iron cylinder mould of 500 x 100 x 100 mm, 100 x 100 x 100 mm, and 100 mm diameter and 200 mm length respectively (that were suitably coated with mould oil). The beam has an effective span to depth ratio of 4 and notch length to depth ratio of 0.2. The width of notch is 2mm. Specimens are demoulded after 24 hours of casting and cured in walk-in stability chamber. The temperature and relative humidity (RH) inside chamber are 27ºC ± 1% and 70 ± 5 % respectively (maintained consistently for 28 days).

2.2.2 Experimental setup

Tests were conducted on digitally controlled closed loop servo-hydraulic universal testing machine controller of 2000 kN and 35 kN for compressive strength and flexural strength respectively. Experimental set up and schematic diagram for compressive strength and split tensile strength are shown in Figure 1. Flexural strength has been conducted using a 3-point bending test on a notched beam specimen and performed under crack mouth opening displacement control (CMOD). The CMOD was mounted across the notch plates.

Table 3: Details of mix design

Name of mix	Fly ash [Kg/m^3]	GGBFS [Kg/m^3]	solutions. [Kg/m^3]	Coarse aggregates [Kg/m^3]		Sand [Kg/m^3]	super-plasticizer [Kg/m^3]	Additional water required [Kg/m^3]
				10 mm	20mm			
Mix2	280	120	200	654.8	436.5	595.3	8	37.038
Mix3	200	200	200	663.4	442.2	601.62	8	37.038

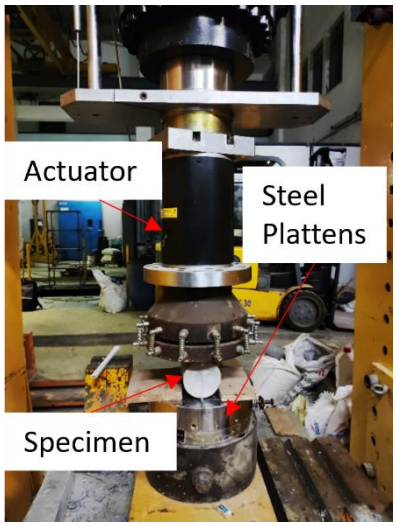

Figure 1: Experimental set-up for the compressive and indirect-tensile strength

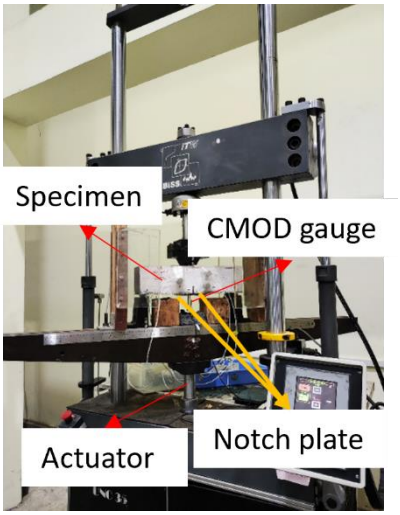

Figure 2: Experimental set-up for 3-point bending test

The test setup and schematic diagram are shown in Figures 2 and 3. All the testing has been conducted at bi-axial fatigue lab, Department of Civil Engineering, Indian Institute of Science Bangalore.

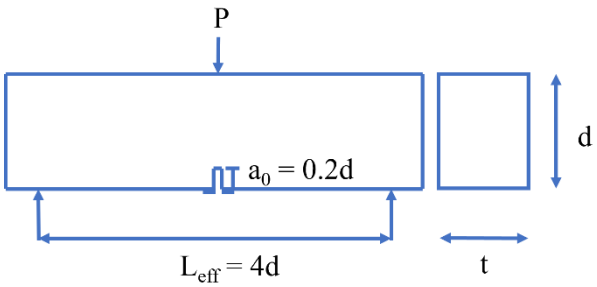

Figure 3: Schematic diagram for 3-point bending test

3 Micro-characterizations of precursors and hardened concrete

Precursors play a significant role in the development of the microstructure of geopolymer concrete. Different techniques were used to study the microstructure of the precursor and the hardened concrete, *viz*, 1) Fourier transform infrared (FT-IR) spectroscopy; 2) X-Ray diffraction (XRD) and 3) Scanning Electron Microscopy (SEM).

3.1 Fourier transform infrared (FT-IR) spectroscopy.

The FT-IR spectra of precursor and geopolymer harden concrete has been recorded in a Shimadzu IR Affinity- 1S instrument and shown in Figure 4, 5 and 6. The bands have been assigned based on previous studies [11], [12] and listed in Table 4. The position of peaks vary due to the type of precursors and the type of mix proportion. The peak for fly ash and GGBFS at 1068 and 908 cm^{-1} respectively represent the asymmetric stretching vibrational bond of Si-O-Si or Si-O-Al. The peaks of geopolymers were obtained at 965 cm^{-1} which is a lower wavenumber than the precursors. This is because of formation of more Si-O-Si or Si-O-Al bond in the network which leads to a

denser structure [13]. Formation of C-A-S-H and N-A-S-H gel results in the decrease of wavenumber which is associated with decrease in the amount of Al [13]. 3400-3650 cm^{-1} zone corresponds to symmetric and asymmetric vibrational stretching of H-OH and 1649 cm^{-1} is related to bending vibration of -OH group of products. These bands are not present in the unreacted fly ash and GGBFS which indicate the occurrence of the geopolymerization reaction [14].

Table 4: Assignment of band

Wavenumber (cm^{-1})	Band assignment
950-1250	Asymmetric stretching vibrational (Si-O-Si and Al-O-Si)
1068	Asymmetric stretching vibrational (Si-O-Si and Al-O-Si)
798	Symmetric stretching vibrational (Si-O-Si)
561	Symmetric stretching vibrational (Al-O-Si)
1650	H-OH bending
3400-3650	-OH, symmetric and asymmetric stretching

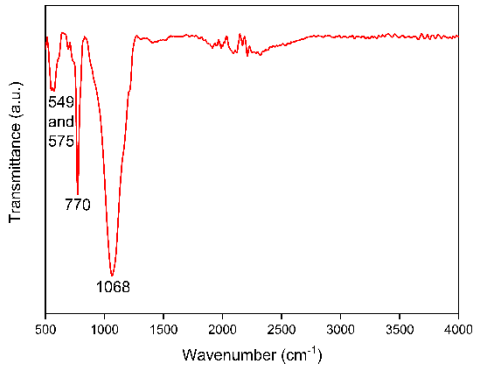

Figure 4: FT-IR of fly ash

3.2 Scanning Electron Microscopy

The surface morphological study of the raw material has been carried out using the ESEM Quanta 200. The microstructure of the precursors, fly ash and GGBFS are shown in Figure 7 and Figure 8 respectively. From Figure 7, it can be concluded that most of the ferrospheres have rough surfaces and are spherical in shape. Ferrospheres in fly ashes can be classified in to smooth ferrospheres, polygon ferrospheres, and granular ferrospheres. Xue *et al*. [10] concluded that polygonal ferrospheres display blocky crystalline surface which is composed of iron oxides and granular ferrospheres possesses a rough, porous, and grainy surface configuration which is frequently further intricate due to the presence of additional granular crystals. From Figure 8, it can be concluded that GGBFS have irregular shape and sharp edges. The glassy nature of GGBFS particles can be observed through SEM. The SEM image of mix-1 geopolymer concrete is shown in Figure 9. The unreacted fly ash, GGBFS and reacted fly ash, GGBFS can be seen. The edge between ITZ and coarse aggregates is shown in the figure.

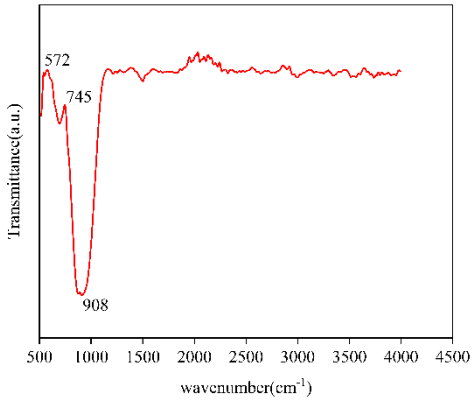

Figure 5: FT-IR of GGBFS

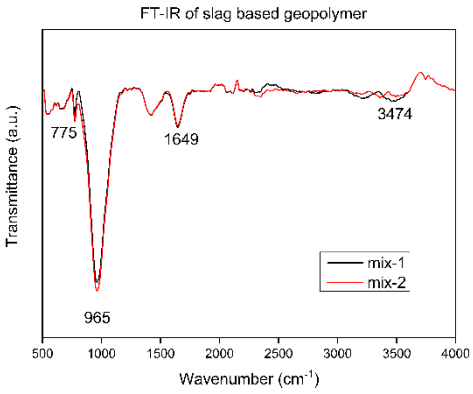

Figure 6: FT-IR of fly ash-GGBFS based geopolymer

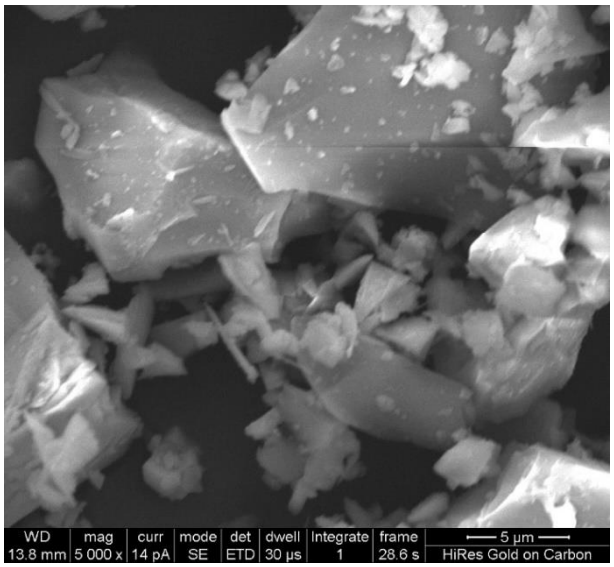

Figure 7: SEM image of GGBFS

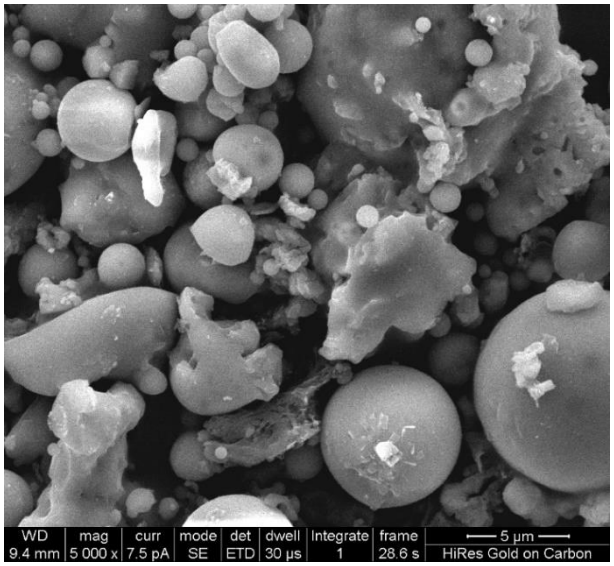

Figure 8: SEM image of fly ash

3.3 XRD

The XRD spectrum of fly ash has been shown in Figure 10. The major peak has been observed at 26.63º which corresponds to the presence of quartz (SiO_2), also supported by XRF (as 59% was detected in fly ash). The next major peak observed is mullite ($3Al_2O_3.SiO_2$) at 31º, 33º, 35º, 60º. The other peaks corresponding to Hematite (Fe_2O_3), Magnetite (Fe_3O_4) are observed at 60 and 40 respectively. Quartz, mullite, magnetite, and Hematite are the main crystalline minerals observed in the fly ash as indicated by a broad hump between 20-28º (2θ).

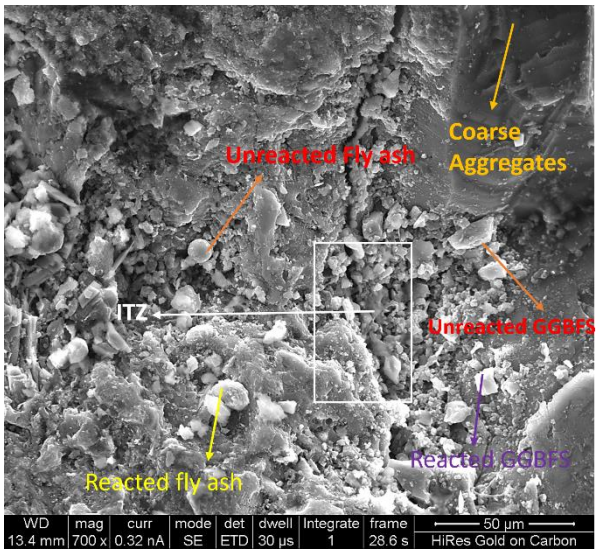

Figure 9: SEM image of geopolymer concrete of mix-1

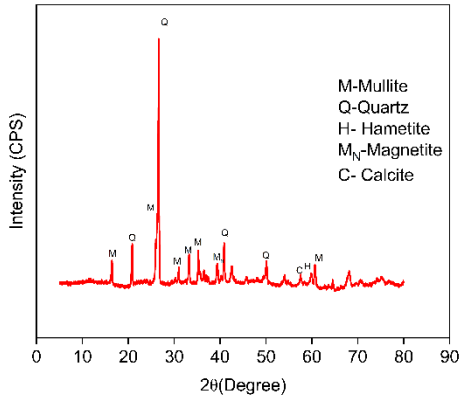

Figure 10: XRD of fly ash

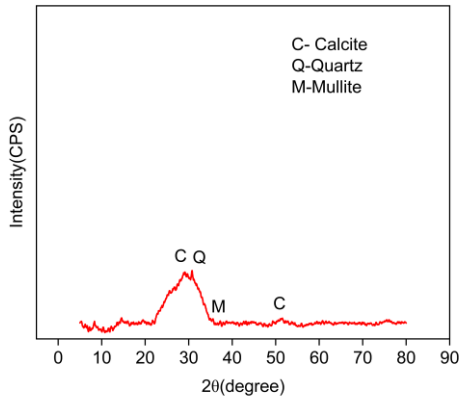

Figure 11: XRD of GGBFS

The XRD spectrum of GGBFS is shown in the Figure 11. The amorphous nature of the GGBFS is observed as broad diffuse hump centred between 22-35º (2θ). The XRD spectrum of GPC mix-1 and mix-2 are shown

in Figure 12 and Figure 13. It is observed that the mullite and Quartz peak remain intact as in precursors even after activation with geopolymer concrete. The amorphous nature is also observed in the XRD patterns of geopolymer concrete as there is a hump between 20-32º. In this hump, amorphous gel peaks exist. New peaks are also observed near 26-30º which are the results of formation of CSH gel products [20].

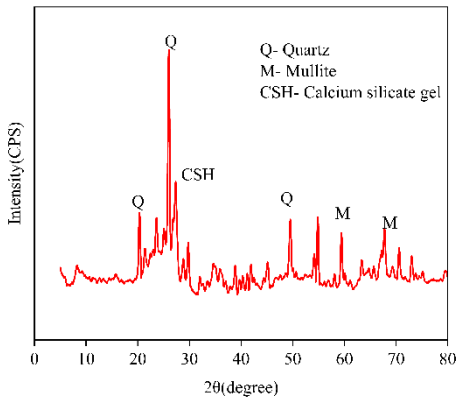

Figure 12: XRD of Mix-1 geopolymer concrete

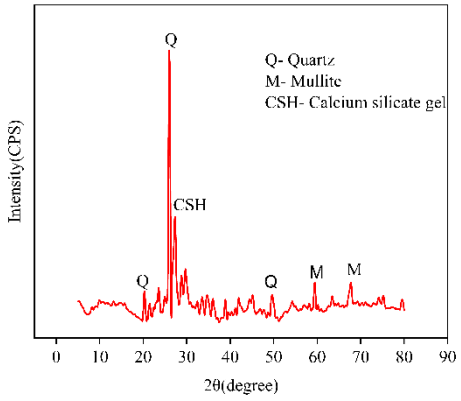

Figure 13: XRD of Mix-2 geopolymer concrete

4 RESULTS AND DISCUSSION

4.1 Fresh and mechanical properties of Geopolymer concrete

The fresh concrete has a greater cohesive and viscous nature. To achieve the workability of geopolymer concrete, we have added superplasticizer and additional water. The slump of geopolymer concrete is listed in Table 5. This achieved value of slump is sufficient for consideration as pumpable concrete. Strength test has been conducted on cube specimen with 2000 kN testing machine. The test is conducted under displacement control with rate of loading 0.24 mm/minute. The 7^{th} and 28^{th} days compressive strength of cube and indirect-split tensile strength of geopolymer concrete is listed in Table 5.

Table 5: Properties of GPC mix-1 and mix- 2

Mix no.	Slump value	FC_7	FC_{28}	Ft_{28}
1	185 mm	43.4	55.6	2.54
2	160 mm	51.1	61.15	3.37

FC_7 -7^{th} day compressive strength FC_{28} -28^{th} day compressive strength, Ft_{28} -28 days split tensile strength.

4.2 Flexure properties of geopolymer concrete

The flexure test is conducted on beam specimen with a testing machine of capacity 35 kN as mentioned above. The test is conducted under monotonically increasing CMOD with the rate of 0.001mm/sec to achieve the pre-peak and post-peak behavior. The load-CMOD curve has been shown in Figure 15. The failure patterns of mix-1 across the cross-section are shown in Figure 14(a) and 14(b). It is observed that both the aggregate and ITZ have failed. It means, that the crack has penetrated into the aggregates as well as propagated through ITZ. The fact that the aggregates are failing, indicates that the formed ITZ possesses enough strength to breach the cracks via the aggregates. Macro pores and meso-micro pores have also been observed as shown in Figure 14(a) and 14(b).

4.2.1 Modulus of rupture

The bending tensile strength has been obtained through a 3-point bending test and the modulus of rupture, ($f_{ct.}$) was calculated as follows:

$$f_{ct} = \frac{3Pl}{2td_{eff}^2}$$

where, d_{eff} = d-a_0, P is peak load, l is the effective span, t is thickness of specimen, d is the depth of specimen, a_0 is the depth of notch. The calculated value of f_{ct} of mix-1 and mix-2 has been shown in Table 6.

Figure 14(a): Cracked surface under 3-point bending test

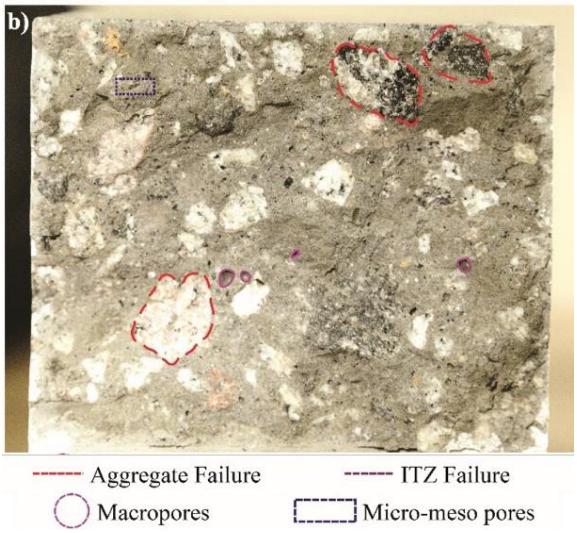

Figure 154(b): Cracked surface under 3-point bending test

Table 6: Calculated value of modulus of rupture

Mix No.	Maximum load (kN)	f_{ct} (MPa)
1	4.2237	3.96
2	4.9798	4.66

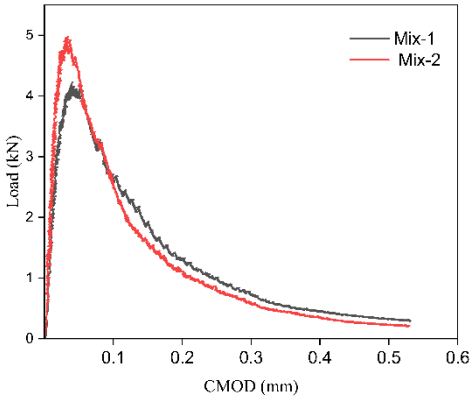

Figure 165: Load-CMOD graph of GPC

4.2.2 Mode-I Critical stress intensity factor (K_{IC})

The fracture toughness K_{IC} is calculated using the linear elastic fracture mechanics (LEFM) approach. This method utilizes the peak load obtained from the 3-point bending test and accounts for the size and shape effects of specimen. K_{IC} is evaluated as follows based on literature reports [15].

$$K_{IC} = \frac{1.5\, P_{max}\ l_{eff}\ \sqrt{\pi a_0}}{t\, d^2} f(\alpha)$$

and

$$f(\alpha) = \left(\frac{0.68 - 0.744\alpha}{1 - 2.155\alpha + 1.16\alpha^2} + 0.36 - 2.088\alpha + 4.611\alpha^2 - 6.499\alpha^3 + 4.232\alpha^4\right)$$

where, P_{max} is the maximum load (N), l_{eff} is the effective span, t is the thickness of specimen, d is the depth of specimen, a_0 is the depth of notch and α is the ratio of depth of notch to effective span i.e., a_0/l_{eff}. The calculated value of K_{IC} of mix-1 and mix-2 has been shown in Table 7.

Table 7:Calculated value of K_{IC}

Mix No.	Maximum load (kN)	K_{IC} (MPa.$m^{1/2}$)
1	4.2237	0.618
2	4.9798	0.748

4.2.3 Fracture energy (G_F) calculation

The fracture energy is calculated as per

RILEM recommendation by TC-FMC.

$$G_F = \frac{A_0 + mg\delta_0}{A_{lig}} = \frac{\int_0^{\delta_0} P(\delta)d\delta + mg\delta_0}{t(d - a_0)}$$

where A_0 (J) is the area under the load-CMOD curve, m (kg) is the mass of the beam between the support, g (m/s^2) is the acceleration due to gravity, δ_0 (μm) is the final midpoint deflection, A_{lig} (m^2) is the ligament area. In this study, A_0 was calculated using the load-CMOD graph instead of load-midpoint deflection graph as done by other researchers [15,16]. This assumes that there exists a linear relationship between midpoint deflection and CMOD in 3-pont bending test based on experimental support [17,18,19]. The calculated value of G_F of mix-1 and mix-2 have been shown in Table 8. Keerthana and Kishan [21] as well as Singh P *et.al* [22] reported that values of G_F of OPC plain concrete are lies in the range of 100 to 130 N/m.

Table 8: Calculated value of G_F

Mix No.	Maximum load (kN)	A_0 (J)	G_F (N mm^{-1})
1	4.227	0.65682	0.082
2	4.9798	0.672	0.084

6 Conclusions

This study experimentally demonstrates the fresh properties of geopolymer concrete, microstructural formation and fracture properties of hardened geopolymer concrete on varying the fly ash to slag content in the mix design. The following conclusions can be drawn from our analysis:

- The proposed mix can achieve the workability of geopolymer concrete. On increasing the slag content, the workability of geopolymer concrete decreases because the GGBFS has more surface area which requires more liquid for workability.
- On increasing the GGBFS content, mechanical properties of geopolymer concrete shows enhancement in the compressive strength, split tensile strength, modulus of rupture, and fracture energy.
- The fracture energy of geopolymer concrete shows generally lower values than OPC concrete.
- The ITZ formed is stronger as the breaking of aggregates takes place.

ACKNOWLEDGEMENT

The author has no competing interests to declare.

REFERENCES

[1] Gartner, E., 2004. Industrially interesting approaches to "low-CO_2" cements. *Cement and Concrete research*, *34*(9), pp.1489-1498..

[2] Davidovits, J.G., 1991. Inorganic polymer new materials. *Journal of Thermal Analysis*, *37*(1), pp.661-663.

[3] Fernández-Jiménez, A. and Palomo, A., 2005. Composition and microstructure of alkali activated fly ash binder: Effect of the activator. *Cement and concrete research*, *35*(10), pp.1984-1992.

[4] Chindaprasirt, P., Chareerat, T. and Sirivivatnanon, V., 2007. Workability and strength of coarse high calcium fly ash geopolymer. *Cement and concrete composites*, *29*(3), pp.224-229.

[5] Hardjito, D., Wallah, S.E., Sumajouw, D.M. and Rangan, B.V., 2004. On the development of fly ash-based geopolymer concrete. *Materials Journal*, *101*(6), pp.467-472.

[6] Olivia, M. and Nikraz, H., 2012. Properties of fly ash geopolymer concrete designed by Taguchi method. *Materials & Design (1980-2015)*, *36*, pp.191-198.

[7] Hewayde, E., Nehdi, M., Allouche, E. and Nakhla, G., 2006. Effect of geopolymer cement on microstructure, compressive strength and sulphuric acid resistance of concrete. *Magazine of Concrete Research*, *58*(5), pp.321-331.

[8] Kupwade-Patil, K. and Allouche, E.N., 2013. Impact of alkali silica reaction on fly ash-based geopolymer concrete. *Journal of materials in Civil Engineering*, *25*(1), pp.131-139.

[9] Ryu, G.S., Lee, Y.B., Koh, K.T. and Chung, Y.S., 2013. The mechanical properties of fly ash-based geopolymer concrete with alkaline activators. *Construction and building materials*, *47*, pp.409-418.

[10] Xue, Q.F. and Lu, S.G., 2008. Microstructure of ferrospheres in fly ashes: SEM, EDX and ESEM analysis. *Journal of Zhejiang University-SCIENCE A*, *9*(11), pp.1595-1600.

[11] Lee, W.K.W. and Van Deventer, J.S.J., 2003. Use of infrared spectroscopy to study geopolymerization of heterogeneous amorphous aluminosilicates. *Langmuir*, *19*(21), pp.8726-8734.

[12] Petrus, H.T.B.M., Adelizar, A.S., Widiyatmoko, A., Olvianas, M., Suprapta, W., Perdana, I., Prasetya, A. and Astuti, W., 2019, May. Kinetics of Fly Ash Geopolymerization using Semi Quantitative Fourier-Transform Infrared Spectroscopy (FTIR); Corr Data. In *IOP Conference Series: Materials Science and Engineering* (Vol. 532, No. 1, p. 012001). IOP Publishing.

[13] Al-Majidi, M.H., Lampropoulos, A., Cundy, A. and Meikle, S., 2016. Development of geopolymer mortar under ambient temperature for in situ applications. *Construction and Building Materials*, *120*, pp.198-211.

[14] Somna, K., Jaturapitakkul, C., Kajitvichyanukul, P. and Chindaprasirt, P., 2011. NaOH-activated ground fly ash geopolymer cured at ambient temperature. *Fuel*, *90*(6), pp.2118-2124.

[15] Zhang, S., Li, Z., Ghiassi, B., Yin, S. and Ye, G., 2021. Fracture properties and microstructure formation of hardened alkali-activated slag/fly ash pastes. *Cement and Concrete Research*, *144*, p.106447.

[16] Standard, J.C.I., 2003. Method of test for fracture energy of concrete by use of notched beam. *JCI-S-001e2003, Japan Concrete Institute*.

[17] Lee, J. and Lopez, M.M., 2014. An experimental study on fracture energy of plain concrete. *International Journal of Concrete Structures and Materials*, *8*, pp.129-139.

[18] Aslani, F. and Bastami, M., 2015. Relationship between deflection and crack mouth opening displacement of self-compacting concrete beams with and without fibers. *Mechanics of Advanced Materials and Structures*, *22*(11), pp.956-967.

[19] Zhao, S., Sun, W. and Lange, D., 2015. Deflection–crack mouth opening displacement relationship for concrete beams with and without fibres. *Magazine of Concrete Research*, *67*(10), pp.532-540.

[20] Mishra, J., Nanda, B., Patro, S.K. and Krishna, R.S., 2022. Sustainable fly ash based geopolymer binders: a review on compressive strength and microstructure properties. *Sustainability*, *14*(22), p.15062.

[21] Keerthana, K. and Kishen, J.C., 2020. Micromechanics of fracture and

failure in concrete under monotonic and fatigue loadings. *Mechanics of Materials*, *148*, p.103490.

[22] Singh, P., Yogesh, R., Bhowmik, S. and Kishen, J.C., 2023. Insights into the fracturing process of plain concrete under crack opening. *International Journal of Fracture*, pp.1-18.